



RESEARCH ARTICLE

Simultaneous realization of time and carrier-envelope phase synchronization for an ultra-intense few-cycle laser pulse coherent combining system

Guoli Zhang^{1,2}, Xiao Liang^{1,2}, Hao Xue^{1,2,3}, Xinglong Xie^{1,2}, Ping Zhu^{1,2}, Fucai Ding^{1,2}, Meizhi Sun^{1,2}, Linjun Li^{1,2}, Rashid Ul Haq^{1,2}, Ailin Guo¹, Xiangbing Zhu³, and Jianqiang Zhu^{1,2}

¹Key Laboratory on High Power Laser and Physics, Shanghai Institute of Optics and Fine Mechanics, Chinese Academy of Sciences, Shanghai, China

²Center of Materials Science and Optoelectronics Engineering, University of Chinese Academy of Sciences, Beijing, China

³School of Physics and Electric Information, Anhui Normal University, Wuhu, China

(Received 21 November 2024; revised 30 January 2025; accepted 2 April 2025)

Abstract

Coherent combining of several low-energy few-cycle beams offers a reliable and feasible approach to producing few-cycle laser pulses with energies exceeding the multi-joule level. However, time synchronization and carrier-envelope phase difference (ΔCEP) between pulses significantly affect the temporal waveform and intensity of the combined pulse, requiring precise measurement and control. Here, we propose a concise optical method based on the phase retrieval of spectral interference and quadratic function symmetry axis fitting to simultaneously measure the time synchronization and ΔCEP between few-cycle pulses. The control precision of our coherent beam combining system can achieve a time delay stability within 42 as and ΔCEP measurement precision of 40 mrad, enabling a maximum combining efficiency of 98.5%. This method can effectively improve the performance and stability of coherent beam combining systems for few-cycle lasers, which will facilitate the obtaining of high-quality few-cycle lasers with high energy.

Keywords: carrier-envelope phase; coherent beam combination; few-cycle pulse; synchronization

1. Introduction

Few-cycle pulse lasers, as a unique category within the family of ultrashort pulse lasers, have garnered increasing attention due to their distinctive characteristics^[1]. As ultrashort lasers tend to reach peak power at several petawatts or even exawatts, few-cycle pulse lasers will naturally benefit from the fact that the same energy can be confined to a shorter temporal duration^[2,3]. When the energy of a few-cycle pulse laser exceeds tens of joules, several novel mechanisms in laser–plasma interactions are unveiled. For instance, proton acceleration driven by an intense few-cycle pulse is particularly advantageous for energy transfer from the laser to the generated ions^[4,5], with a proton cutoff energy greater than GeV being predictable under an instability-free

acceleration regime. Similarly, the energy conversion efficiency of laser-to-electron beams has been shown to improve with laser wake field acceleration using few-cycle high-power lasers^[6,7]. Beyond applications in high-energy-density science, the diverse waveforms of few-cycle pulse lasers introduce a new dimension to the study of intense laser field interactions with matter^[8]. This capability arises from the fact that the electric field shape of a few-cycle pulse is strongly influenced by the carrier-envelope phase (CEP), enabling precise control of atomic-scale electronic motion^[9–11]. The prospect of using a petawatt-class few-cycle laser with a controlled electric field shape in studies of intense laser–matter interactions is both highly intriguing and promising.

However, obtaining petawatt few-cycle laser pulses remains a significant challenge. Although the peak power of ultrashort pulse laser systems based on chirped-pulse amplification (CPA) or optical parametric chirped-pulse amplification (OPCPA) technology can reach up to 10 PW^[12–14], their pulse durations are generally greater

Correspondence to: X. Liang and X. Xie, Key Laboratory on High Power Laser and Physics, Shanghai Institute of Optics and Fine Mechanics, Chinese Academy of Sciences, Shanghai 201800, China. Emails: lx62@siom.ac.cn (X. Liang); xiexl329@siom.ac.cn (X. Xie)

than 20 fs. Recently, the post-compression technique was demonstrated to be applicable to a petawatt-class CPA/OPCPA laser by using a thin-film compressor^[15]. Bleotu *et al.*^[16] reported the successful spectral broadening of a 7 J/21.5 fs laser to a bandwidth compatible with a 15 fs pulse, indicating the feasibility of achieving few-cycle pulses in the PW class. Parametric waveform synthesis, by coherently combining laser pulses with different amplified spectra, is another promising technique for obtaining high-power few-cycle or even single-cycle laser pulses with the ability to tailor optical waveforms. A sub-millijoule and sub-cycle (pulse width of 2.8 fs, 0.6 optical cycles at a central wavelength of 1.4 μm) laser pulse was generated by utilizing a parametric waveform synthesis technique^[17]. Nonetheless, to generate few-cycle ultrashort pulses with higher power, significant technical challenges remain in the post-compression and parametric waveform synthesis. Here, we propose a direct approach to further increase the peak power of few-cycle lasers, that is, few-cycle pulse coherent combination (FCPCC).

Coherent beam combination can greatly increase laser power far beyond what can be achieved with a single laser and has become a common technique in fiber and diode lasers^[18]. While relatively few studies are currently being conducted on FCPCC, two key issues can be foreseen that will seriously deteriorate the combining efficiency of FCPCC. Firstly, time synchronization and spatial beam pointing are notoriously critical factors in coherent combination, in which time synchronization is more destructive because few-cycle pulses have an extremely narrow pulse duration – typically less than five optical cycles. Secondly, and more importantly, coherent combining arises from the interference between the fields of parent few-cycle pulses, and the carrier-envelope phase difference (ΔCEP) between them dramatically deforms the combined laser field. For example, with a CEP shift of π , two pulses will cause destructive interference with the smallest intensity. As an optical pulse propagates through a dispersive material, the CEP evolves due to the difference between phase and group velocities. Consequently, for amplified high-energy few-cycle pulses to be coherently combined, the ΔCEP originates from material thickness variations and refractive index changes caused by inhomogeneities or thermal effects in the amplifier. These factors indicate that minimizing both the time delay and ΔCEP between combined laser pulses is essential for producing stable combined waveforms. Moreover, the deformation of coherent combined pulse waveforms can be very similar when a time delay and ΔCEP appear, making it difficult to distinguish them directly from the retrieved combined light fields^[19]. There are methods to control these two parameters individually, such as balanced cross-correlation (BOC)^[20] for timing jitter and fundamental-to-second-harmonic self-referencing (f-2f)^[21] for CEP stabilization. However, in

an FCPCC system, implementing f-2f measurements and adjustments for ΔCEP at the final stage of every laser channel would introduce excessive complexity.

In this paper, we present a spectral interference (SI)-based phase difference retrieval method for FCPCC, capable of simultaneously measuring the time delay and ΔCEP with high precision. Our method achieves a time delay measurement resolution of 12 as and controls the standard deviation (STD) of the time delay synchronization within 42 as. The ΔCEP is measured with an accuracy better than 40 mrad. The experimental implementation demonstrates FCPCC of two laser channels, with real-time feedback control of both the time delay and ΔCEP .

2. The theory of time delay and carrier-envelope phase difference retrieval

As a linear technique of phase measurement, SI is sensitive and reliable to detect subtle changes between two laser pulses^[22]. The theory of SI can be simply described by $I(\omega) = A_1^2 + A_2^2 + 2A_1A_2 \cos(\Phi(\omega))$, in which $\Phi(\omega)$ is their phase difference. The time delay and ΔCEP are the two main phase terms in $\Phi(\omega)$. Consequently, the interferogram of the SI is highly sensitive to these parameters, and variations in $\Phi(\omega)$ can be directly retrieved from the changing fringes of the interferogram. A common method for extracting the time delay from $\Phi(\omega)$ is the Fourier transform algorithm^[23]. However, this method is better suited for recovering a time delay longer than the pulse duration, as it avoids overlap of the individual autocorrelation term and interference term when applying the inverse Fourier transform to the spectral interferogram. For FCPCC, the time delay between combined pulses must be minimized to approach zero. In our proposed method, the phase difference is directly retrieved by taking the arccosine of $\cos(\Phi(\omega))$, and the resulting phase difference is subsequently fitted using a quadratic function of ω .

Assuming the central frequency of two pulses is ω_0 , they can be represented in the frequency domain as follows:

$$\begin{aligned} E_1(\omega) &= A_1(\omega) e^{i\varphi_1(\omega)}, \\ E_2(\omega) &= A_2(\omega) e^{i(\varphi_2(\omega) + \omega\tau)}, \end{aligned} \quad (1)$$

where $A_1(\omega)$ and $A_2(\omega)$ are the amplitude spectra of the pulses, $\varphi_1(\omega)$ and $\varphi_2(\omega)$ are the phase spectra and τ represents the time delay between the two pulses. For chirped pulses, the phase spectra can typically be expanded using a quadratic polynomial:

$$\begin{aligned} \varphi_1(\omega) &= \varphi_1(\omega_0) + \text{GD}_1(\omega - \omega_0) \\ &\quad + \frac{1}{2} \text{GDD}_1(\omega - \omega_0)^2 + o(\omega^3), \\ \varphi_2(\omega) &= \varphi_2(\omega_0) + \text{GD}_2(\omega - \omega_0) \\ &\quad + \frac{1}{2} \text{GDD}_2(\omega - \omega_0)^2 + o(\omega^3). \end{aligned} \quad (2)$$

Here, $\varphi_1(\omega_0)$ and $\varphi_2(\omega_0)$ denote the carrier phase shifts, GD_1 and GD_2 represent the group delays (GDs), GDD_1 and GDD_2 denote the group delay dispersion (GDD) and $o(\omega^3)$ is referred to as high-order dispersion, which has a relatively minor impact on the calculation compared to GDD. Therefore, it can be neglected during the formula derivation process. However, achieving higher measurement accuracy requires precise correction of the bias introduced by third-order dispersion (TOD). For further details, please refer to the [Supplementary Material](#). Then we can get the following:

$$\begin{aligned} \Phi(\omega) = & \frac{1}{2} \Delta GDD \cdot \omega^2 + (\Delta GD - \tau - \Delta GDD \cdot \omega_0) \omega \\ & + \frac{1}{2} \Delta GDD \cdot \omega_0^2 + \Delta \varphi_0 - \Delta GD \cdot \omega_0, \end{aligned} \quad (3)$$

where $\Delta \varphi_0 = \varphi_1(\omega_0) - \varphi_2(\omega_0)$, $\Delta GD = GD_1 - GD_2$, $\Delta GDD = GDD_1 - GDD_2$. The above expression shows that when $\Delta GDD \neq 0$, $\Phi(\omega)$ is a quadratic function of ω . Since ΔGD represents the GD, combining ΔGD with τ yields the actual time delay:

$$t_d = \Delta GD - \tau. \quad (4)$$

According to the basic properties of a quadratic function, there is a symmetry axis as follows:

$$\omega_s = \frac{\Delta GDD \cdot \omega_0 - t_d}{\Delta GDD}. \quad (5)$$

Thus, the actual time delay between the two pulses can be solved from the symmetry axis as follows:

$$t_d = \Delta GDD \cdot (\omega_0 - \omega_s). \quad (6)$$

It is obvious that ω_s is linearly related to t_d at the symmetry axis, and $t_d = 0$ when $\omega_s = \omega_0$. Here, ΔGDD is obtained directly from the coefficient of the quadratic term of the fitted phase expression. From [Equation \(3\)](#), when $t_d = 0$, we have the following:

$$\Phi(\omega_0) = \Delta \varphi_0 - \Delta GD \cdot \omega_0. \quad (7)$$

Since the CEP refers to the phase difference between the carrier and the envelope:

$$\begin{aligned} \varphi_{1, CEP} &= \varphi_1(\omega_0) - \omega_0 \cdot GD_1, \\ \varphi_{2, CEP} &= \varphi_2(\omega_0) - \omega_0 \cdot GD_2. \end{aligned} \quad (8)$$

Thus, the ΔCEP between the two pulses is as follows:

$$\Delta CEP = \varphi_{1, CEP} - \varphi_{2, CEP} = \Phi(\omega_0). \quad (9)$$

The above derivation demonstrates that for two pulses with GDD differences, the time delay between the two pulses can be determined by analyzing the parabolic characteristics of the SI phase. By further adjusting the time delay to zero, the phase value of the central frequency of the pulse corresponds to the ΔCEP between the two pulses.

Consequently, both the time delay and ΔCEP can be simultaneously resolved, enabling the realization of time and CEP synchronization. Indeed, ΔGDD is necessary and the key point in this method because the function of $\Phi(\omega)$ is quadratic only when there is ΔGDD between two laser beams. In an FCPC system, ΔGDD naturally arises because the pulse duration must be stretched by dispersion components and pass through the OPCPA to achieve energy amplification. This condition also indicates an advantage of our method in that the time delay and ΔCEP can be measured and controlled before dispersion compensation.

3. Experiment: FCPC of two few-cycle laser beams

An FCPC system consisting of two few-cycle pulses was demonstrated to verify the proposed measurement method for the time delay and ΔCEP . As shown in [Figure 1](#), the laser seed was a commercial Ti:sapphire mode-locked femtosecond laser, delivering 10 fs pulses with 20 nJ of energy at a central wavelength of 800 nm. This pulse duration corresponds to approximately four optical cycles. The laser pulse was split into two channels by a 50/50 beam splitter. The transmission channel (designated as channel 1) from the splitter had an additional dispersion and an altered CEP. The CEP of channel 1 was further actively controlled by passing through a wedge pair, where one wedge was mounted on a moving stage driven by a direct current (DC) motor to precisely adjust the wedge thickness. The wedge pair, made of fused silica, had a wedge angle of 1 mrad. In addition to introducing a difference in CEP, the movement of the wedge also introduced changes in the time delay between channels 1 and 2. In our setup, the closed-loop control precision of the piezo-driven delay (PZD) line is 0.6 nm. Specifically, we used the NFL5DP20S/M model from Thorlabs, paired with a KPC101 controller, both of which are well-suited for high-precision applications. The coherent combination of the two laser channels, implemented in a tiled-aperture configuration, was achieved using an off-axis parabolic (OAP) mirror with a focal length of 381 mm. Before combination, the dispersion of the two laser pulses was compensated by chirped mirrors. As shown in [Figure 2](#), the pulse durations of the two channels were measured by a frequency-resolved optical gating (FROG) system to be 10.4 and 10.9 fs, respectively. These results confirm that the two pulses used for coherent combining were indeed few-cycle pulses, corresponding to approximately four optical cycles at a wavelength of 800 nm. To a large extent, in terms of time delay, dispersion and CEP, our experimental setup can

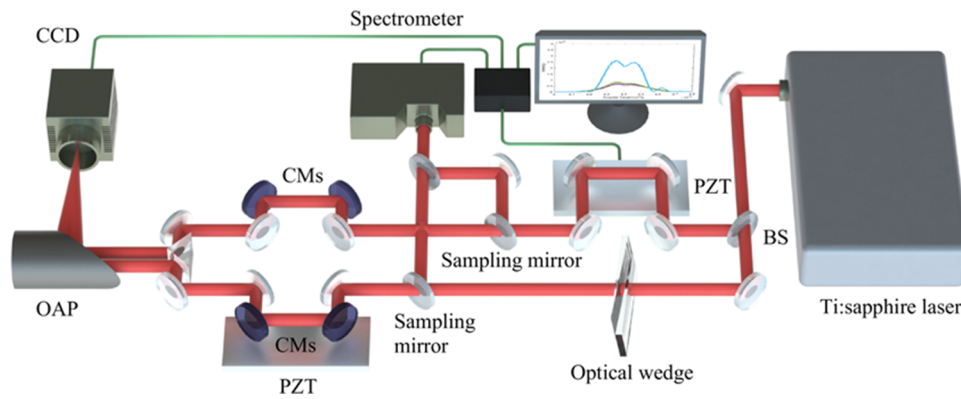


Figure 1. Experimental setup of the FCPCC with an SI system for the measurement of time synchronization and Δ CEP. A commercial Ti:sapphire mode-locked femtosecond laser provided 10 fs pulses with 20 nJ of energy at a central wavelength of 800 nm. The laser pulse was split by a 50/50 beam splitter (BS), where laser channel 1 passed through a wedge pair for active CEP control, while laser channel 2 passed only through a time delay controller mounted on a PZD stage. Both laser channels were sampled for phase difference measurements based on spectral interference. The remaining portions of the lasers were coherently combined in a tiled-aperture configuration, and the far-field interferogram was captured using a CCD camera. Before combination, the two channels passed through chirped mirrors (CMs) for dispersion compensation.

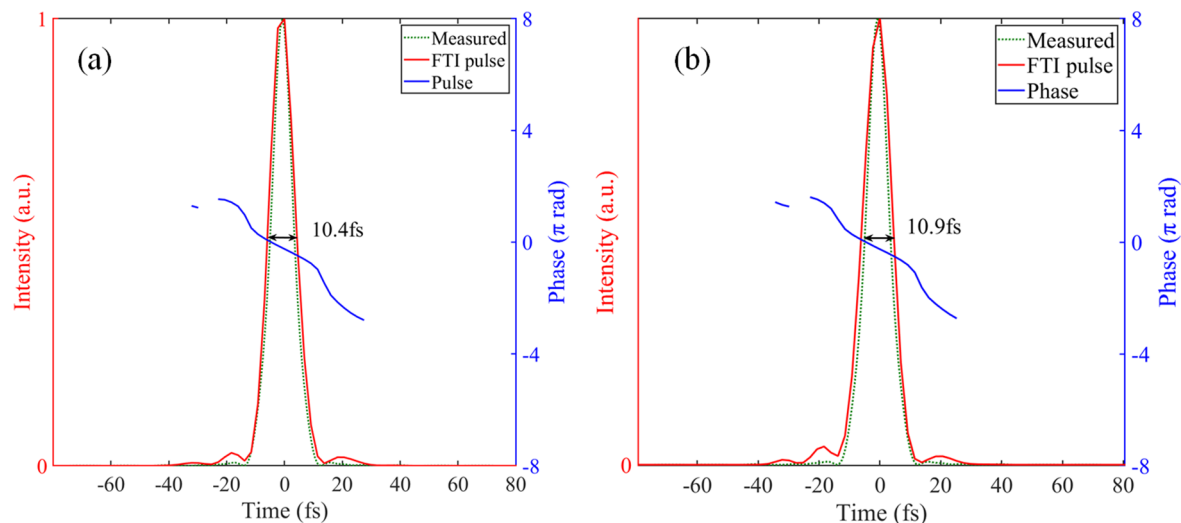


Figure 2. Measured pulse durations of the two laser channels. (a) The pulse duration of channel 1 is 10.4 fs. (b) The pulse duration of channel 2 is 10.9 fs. Both pulse durations correspond to approximately four optical cycles at a central wavelength of 800 nm. The Fourier transform limits according to the spectrum are 9.3 fs for both channels, as shown by the dotted lines.

simulate the actual situation of coherent combination of two high-energy few-cycle pulses. Moreover, in the high-energy few-cycle system, a grating-based compressor is typically required for the dispersion compensation as it can offer large amount of GDD. However, the grating compressor also introduces fluctuations in the CEP. To obtain Fourier transform limits pulses, chirped mirror pairs are necessary to provide accurate dispersion compensation. Our Δ CEP measurement can be implemented between these two stages, allowing control over the CEP fluctuations introduced by the grating compressor.

The SI was implemented using a Mach–Zehnder interferometer, as shown in Figure 1. The two interference arms were sampled from laser channels 1 and 2 and recombined in a collinear geometry through a beam splitter. The interferogram produced by the SI was collected by a spectrometer

(Ocean Optics, HR4000+). The data were analyzed using a quadratic function fitting method to extract the time delay and Δ CEP, which were subsequently fed back to the PZD and DC motor for active control of these two parameters. Figure 3 presents the spectral interferogram and the retrieved phase difference of two laser pulses at different time delays. Although the retrieved phase difference (orange curve) is not phase unwrapped, a quadratic curve (red curve) can still be fitted in all cases. The symmetry axis ω_s of the fitted quadratic curve (blue dotted line) determines the angular frequency difference ($\Delta\omega$) between ω_s and ω_0 . Omitting the phase unwrapping step reduces the computation time for solving the time delay. Using Equation (6), the time delays shown in Figure 3 were determined to be 1.31, 4.85 and 24.10 fs, respectively. As ω_s approaches ω_0 , the time delay decreases. When $\Delta\omega$ is less than the fitting resolution of our

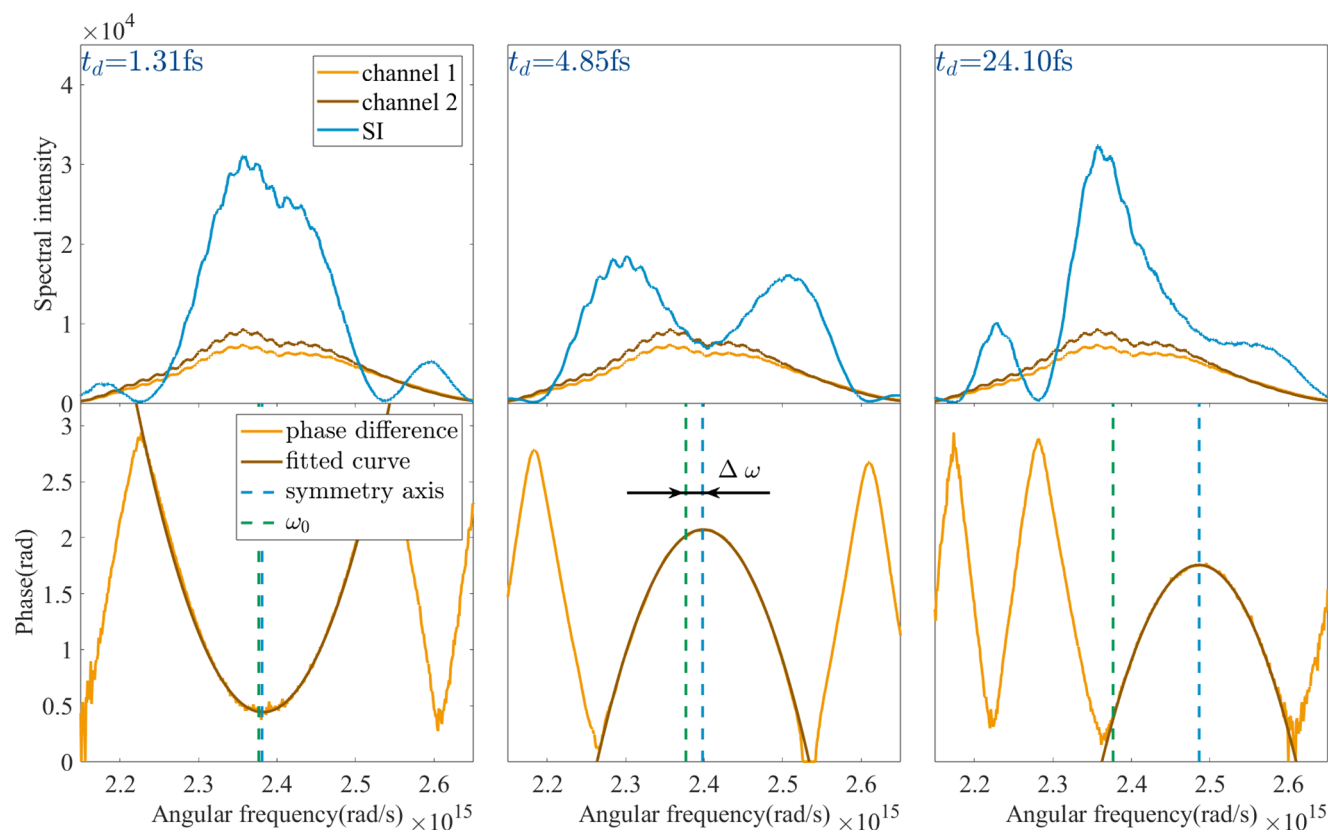


Figure 3. Spectral interferogram and retrieved phase difference of two laser pulses at different time delays. Each retrieved phase difference (orange curve) from the spectral interferogram is fitted with a quadratic curve (red curve). The symmetry axis (blue dotted line) determines the angular frequency difference $\Delta\omega = \omega_0 - \omega_s$, from which the time delay (t_d) can be calculated.

SI method, the time delay is considered to be zero, indicating that the two laser pulses are time synchronized. The spectral resolution of the spectrometer used in our setup is 0.2 nm. Our measurement method achieves a temporal resolution of 12 as, with further analysis provided in Section 4 and the Supplementary Material.

Subsequently, the ΔCEP can be determined using Equation (2). When the time delay t_d is equal to zero, the retrieved phase difference $\Phi(\omega_s)$ corresponds to ΔCEP . Figure 4 presents the spectral interferogram for this condition, where all the symmetric axes of the quadratic fitted curves align with the central frequency ω_0 . Here, ΔCEP values of 0.027, 1.534 and 2.950 rad were measured for three different interferograms, as shown in Figure 4. Without active feedback control, environmental disturbances – such as mechanical vibrations and air currents – caused significant time delay drifts, as shown in Figure 5(a). These drifts led to a loss of temporal stability, with large fluctuations observed over time. Engaging the active feedback system effectively suppressed low-frequency noise components, as shown by the reduced time delay fluctuations in the latter portion of Figure 5(a) and the corresponding frequency spectrum in Figure 5(b).

To further validate our ability to precisely measure and control ΔCEP , the wedge thickness was adjusted to span the ΔCEP across a range of π in our experiment, with

the measurement results depicted as the orange signal in Figure 6. The optical wedge was adjusted by 1 mm every few minutes while maintaining time synchronization (blue signal). Each step of wedge adjustment induced a measured variation in ΔCEP of approximately 0.105 rad. Starting at -1.72 rad, ΔCEP reached 2.28 rad after 38 adjustments. Both the blue and orange signals exhibit fine spikes, representing instantaneous changes in the time delay and ΔCEP detected during incremental adjustments of the wedge thickness by the DC motor. Abrupt changes in the time delay were immediately corrected by the feedback system. During prolonged feedback stabilization, the STD of the time delay was effectively controlled to within 42 as.

With the control of the ΔCEP while keeping time synchronized, we observed the FCPCC using a charge-coupled device (CCD) camera. Spatial interference fringes formed in the far-field due to the tiled-aperture configuration. Notably, this configuration of FCPCC is highly efficient, as it avoids energy loss and potential damage to the combining mirrors, making it suitable for high-energy systems at the hundred millijoule or joule level. Laboratories aiming to achieve exawatt-class lasers through the coherent combination of petawatt lasers predominantly employ tiled-aperture configuration^[24,25]. Figure 7(a) shows the central cross-section of the far-field interference fringes for varying ΔCEP values.

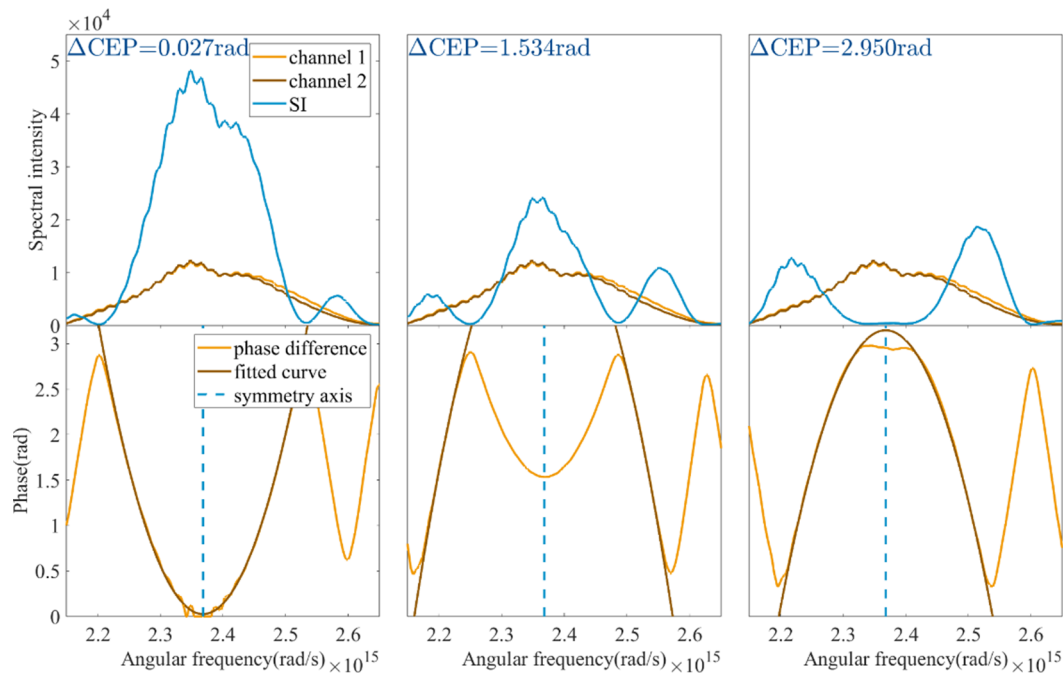


Figure 4. Spectral interferogram and retrieved phase difference of two synchronized laser pulses at different ΔCEP values. When the symmetry axis ω_s of the quadratic curve aligns with ω_0 , t_d is determined to be zero; then, the retrieved phase difference at the symmetry axis corresponds directly to the ΔCEP .

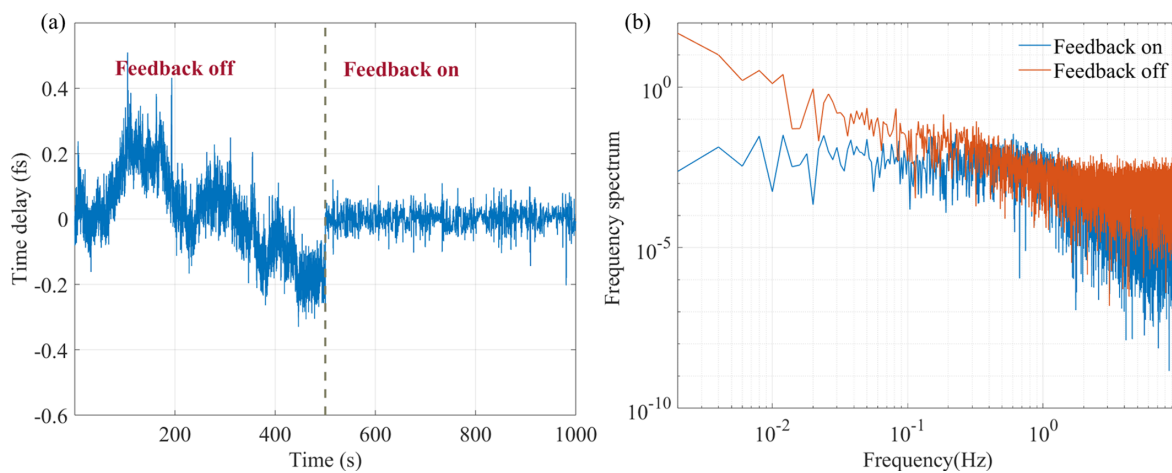


Figure 5. Time delay stability (a) and jitter power spectrum (b) with feedback on and off.

As the ΔCEP is varied, the strongest fringe gradually shifts, demonstrating the linear movement of interference fringes. This result confirms that the measurement and regulation of the ΔCEP were effectively achieved based on time synchronization through SI. To further characterize the FCPC performance, we calculated the combining efficiency for each ΔCEP value and compared it with numerical simulations based on the angular spectrum method. The combining efficiency is defined as the ratio of the focused peak intensity of the combined beam to the maximum achievable value under perfectly coherent conditions^[26]. As shown in Figure 7(b), the experimental combining efficiency (solid line) aligns very well with the simulated efficiency (dashed line). The highest combining efficiency, approximately 98.5%, is

reached for $\Delta\text{CEP} = 0$ (blue dot c), while the efficiency drops to 85.6% when $\Delta\text{CEP} = \pi$ (blue dot e). The highest combining efficiency does not reach 100% because of a measured ΔGDD of 5 fs² between the two combined pulses, which also accounts for the slight differences in pulse durations shown in Figure 2. Notably, the relative ΔCEP measured in the SI setup shown in Figure 1 differs from the actual ΔCEP in the far-field combined beam. However, the relative phase difference between these two positions remains constant, and we initially calibrated the phase difference and time delay using the same SI method. Detailed information on calibration can be found in the Supplementary Material. The relative phase difference of ΔCEP in our experiment was determined to be 1.5 rad.

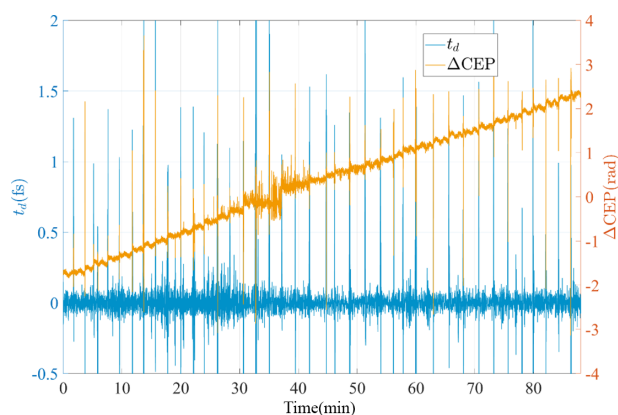


Figure 6. Measurement results of continuously varying ΔCEP s within a range larger than π while maintaining time synchronization. The blue signal represents the measured time delay, and the orange signal represents the measured ΔCEP . The spikes observed in both signals correspond to instantaneous changes in the time delay and ΔCEP , detected during incremental adjustments of the wedge thickness.

In addition, minor modifications to the experimental setup in Figure 1 enabled beam combining in a filled-aperture configuration. A beam splitter sampled the combined pulse entering the spectrometer and directed a portion to a CCD camera for focal spot intensity monitoring. Employing the same experimental procedure as in Figure 7(a), we observed the combined beam profile behavior depicted in Figure 7(f). In this configuration, as the two pulses co-propagate axially, no fringe movement was observed. Instead, significant intensity modulation occurred in the combined focal spot. The ΔGDD between the combined pulses was measured to be approximately 220 fs^2 . This relatively high ΔGDD produced variations in combining efficiency ranging from 20% to 80%, in strong agreement with our simulations, as illustrated in Figure 7(g). These experimental results reveal that in far-field coherent combining, a noncollinear configuration is more robust against ΔCEP variations compared to a collinear configuration, which results in destructive interference when $\Delta\text{CEP} = \pi$. However, the ΔCEP can still cause approximately 15% efficiency decline. The experimental results from Figures 6 and 7 demonstrate the precise ΔCEP control in both configurations, while simultaneously ensuring accurate time synchronization.

4. Discussion

The accuracy of the ΔCEP measurements was evaluated by comparison with the theoretical values derived from the experimental setup. The dotted blue line in Figure 8 represents the theoretical ΔCEP variation induced by translating the optical wedges. In the experiment, when the wedge is displaced by 1 mm, the thickness changes by $1 \mu\text{m}$ due to its wedge angle of 1 mrad. Based on the data in Figure 6, the mean value of the measured ΔCEP at each step is fitted

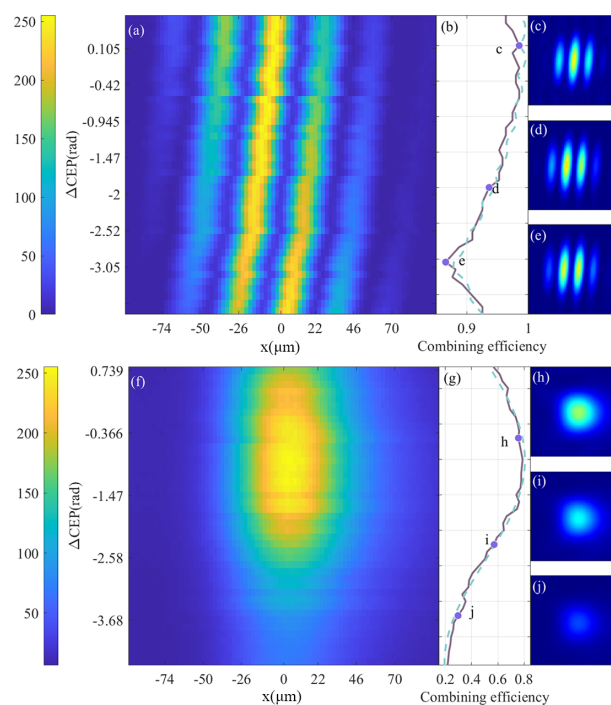


Figure 7. Far-field interference fringes and efficiency obtained for FPCPC under different ΔCEP values in the tiled- (a) and filled-aperture (f) configurations. The strongest interference fringe in Figure 7(a) gradually shifts with increasing ΔCEP , and the highest combining efficiency (98.5%) is reached only when $\Delta\text{CEP} = 0$. For the filled-aperture configuration in Figure 7(f), there is no interference fringe, and the maximum beam combining intensity is also reached when $\Delta\text{CEP} = 0$. The solid lines in Figures 7(b) and 7(g) show the experimentally obtained combining efficiency, while the dashed lines correspond to the simulation results based on the experimental parameters. In addition, Figures 7(c)–7(e) and 7(h)–7(j) depict the spatial interference patterns observed at three distinct ΔCEP values identified on the efficiency curves in Figures 7(b) and 7(g), respectively. These patterns further illustrate the dependence of the combining performance on the ΔCEP for each configuration.

to produce the green line in Figure 8, and the measurement STD is shown as a gray line. The ΔCEP measurement shows good agreement with the ideal linear relationship dictated by the optical wedge thickness variation, as evident in Figure 8. The fused silica wedge used in the experiment exhibits minimal surface profile error, enabling the thickness variation to be treated as ideal and linear, resulting in a corresponding ΔCEP variation that is also linear. Surface profile measurements of the wedge, detailed in the Supplementary Material, confirm that its contribution to the overall error is negligible. For a laser pulse with a central wavelength of 800 nm, a thickness variation of $1 \mu\text{m}$ corresponds to a ΔCEP change of approximately 107 mrad.

Our measurement results show a ΔCEP variation of $105 \text{ mrad}/\mu\text{m}$, which aligns closely with the intrinsic material parameter of $107 \text{ mrad}/\mu\text{m}$ with an error below 2%. The mean STD of the ΔCEP measurements is about 40 mrad at points farther from $\Delta\text{CEP} = 0$ rad, demonstrating the good accuracy and stability of our method in these regions. However, the STD increases significantly near

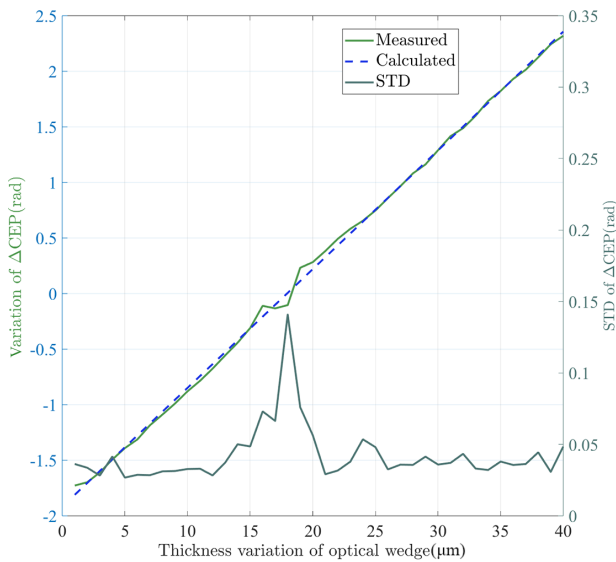


Figure 8. Comparison of the variation in ΔCEP between the measured results and theoretical values. The dotted blue line represents the theoretical ΔCEP variation induced by wedge translation, while the green line is fitted to the mean measured ΔCEP values at each step of Figure 5. The gray line represents the STD of each measurement, in which the mean STD is 40 mrad.

$\Delta\text{CEP} = 0$ rad, reaching approximately 140 mrad, due to higher sensitivity to time delay jitter in this region. When the repetition rate of the laser pulse far exceeds the spectrometer's acquisition frequency, the SI signal represents the cumulative result of multiple interferences. Consequently, the calculated spectral phase difference reflects an averaged value over the acquisition cycle, which prevents complete constructive or destructive interference, as shown by the solid line in Figure 9. To examine this, simulations incorporating time delays and TOD were compared with experimental data. As shown in the results, the spectral phase difference between the two pulses was distorted at 0 and π . By adding random time delay jitter (0.15 fs) to simulate the spectrometer's integration process, the noisy simulated phase φ_{noise} closely matched the experimental results φ_{exp} , compared to the phase φ_{ideal} under ideal conditions, as illustrated by the chain line in Figure 9, confirming that the incomplete interference originates from spectrometer averaging. As shown in Figure 4, under the same experimental conditions, when $\Delta\text{CEP} = 2.95$ rad, more pronounced phase distortion is observed near the central frequency. To further reduce measurement deviation, achieving shorter exposure times and enhanced mechanical stability is highly necessary.

In the experiment, we calculate the time delay by fitting a quadratic function to the spectral phase difference to obtain the symmetry axis ω_s , which is subsequently solved according to Equation (6). Given the exceptional stability of ΔGDD , the resolution of the fit to the symmetry axis directly determines the resolution of the time delay. The spectrometer

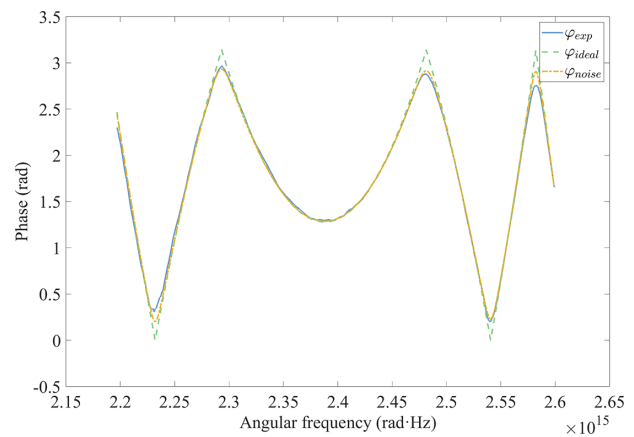


Figure 9. Experimental spectral phase difference (solid line) and noisy simulated phase (dashed line) considering the impact of the time jitter of multiple pulses.

used in the setup has a pixel resolution of 0.2 nm. To balance computational accuracy and efficiency, 10 points are selected from the phase data for each fit, and the symmetry axis resolution is determined to be 55 GHz using the error propagation method. Furthermore, the corresponding temporal delay resolution can be calculated using Equation (6), yielding a value of approximately 12 as. Detailed calculations are provided in the Supplementary Material.

By substituting Equations (4), (6) and (8) into Equation (7), we obtain the following formula when $\omega = \omega_0$:

$$\Delta\text{CEP} = \Phi(\omega_0) - \omega_0 \cdot t_d. \quad (10)$$

This is the formula we used to obtain the ΔCEP values in our experiment. Under the current experimental conditions, when the optical wedge remains stationary, ΔCEP is relatively stable. Therefore, variations in ΔCEP are primarily caused by changes in the phase at the central frequency and the time delay. We use the following error propagation formula:

$$\sigma(\Delta\text{CEP}) = \sigma(\Phi(\omega_0)) + \omega_0 \cdot \sigma(t). \quad (11)$$

In our current experiment, only a single spectrum was collected before the interference of the two pulses, making it necessary to consider the impact of light source power stability on the measurements. Since $\Phi(\omega_0) = \arccos\left(\frac{I_1 - I_2}{2\sqrt{I_1 I_2}}\right)$, the error propagation formula can be expressed as follows:

$$\sigma(\Phi(\omega_0)) = \frac{\sigma_I}{2\sqrt{I_1 I_2} \sqrt{1 - \cos^2 \Phi(\omega_0)}}. \quad (12)$$

From the above equation, it can be observed that $\Phi(\omega_0)$ exhibits greater uncertainty at 0 or π . This, in turn, explains why a measurement deviation of 140 mrad was observed when $\Delta\text{CEP} = 0$. To achieve the optimal resolution of the

system, measurement points near $\cos(\Phi(\omega_0)) = 0$ should be selected, as the error amplification factor is minimized and the system resolution is maximized at this condition. At this point, $\Phi(\omega_0) = \pi/2$. The spectral integration time was 10 ms, corresponding to a spectral energy fluctuation $\sigma_1 = 0.5\%$, which is relatively small and stable. A 0.5% fluctuation in light intensity will induce an approximately linear variation in $\sigma(\Phi(\omega_0))$. Then, we calculated $\sigma(\Phi(\omega_0)) = 5$ mrad. Given that $\omega_0\sigma(t_d) = 28$ mrad, the measurement resolution of ΔCEP is determined to be 33 mrad. The current measurement precision is already approaching the resolution limit of the system under the present experimental conditions. By increasing the number of sampling points and real-time monitoring of light source fluctuations, it is possible to further improve the measurement resolution and system stability. However, this improvement comes at the cost of significantly longer computation times and higher operational expenses. Therefore, in practical applications, a balance must be struck between feedback speed and precision. We cannot further control these errors in our experiments because the speed of our feedback loop is much slower than the frequency of the errors; in other words, the upper bandwidth limit of our feedback loop is 100 Hz, which is mainly restricted both by the response time of the PZD and the acquisition frequency of the spectrum meter.

5. Conclusion

In conclusion, we proposed a method for generating high-energy few-cycle laser pulses through the coherent combination of low-energy pulses, using a concise optical approach based on SI to simultaneously synchronize time delay and CEP. Without involving nonlinear optical processes, this method has quite a low requirement for laser energy, which makes it possible to integrate these measurements on a chip-based spectrometer^[27,28]. In addition to a few-cycle laser, the time delay measurement and control can be extended to femtosecond lasers and picosecond lasers. Notably, this method remains robust and scalable when applied to high-energy few-cycle pulse systems. Its ability to perform single-shot spectral sampling for each pulse eliminates measurement errors caused by energy fluctuations, which is critical for the coherent combination of amplified lasers with lower repetition rates. In the next step of our work, this method will be exploited in the coherent combination of several amplified few-cycle lasers with tens of millijoule energy, which can further push the energy of few-cycle laser pulses to the joule level.

Supplementary material

The supplementary material for this article can be found at <http://doi.org/10.1017/hpl.2025.33>.

Acknowledgements

This work is supported by the Key Projects of Intergovernmental International Scientific and Technological Innovation Cooperation (Grant No. 2021YFE0116700), the National Natural Science Foundation of China (NSFC) (Grant Nos. 12204500 and 12074399), the Shanghai Sailing Program (Grant No. 22YF1455300) and the Chinese Academy of Sciences (Grant Nos. XDA25020105, XDA25020103 and XDA25020101).

References

1. J. A. Wheeler, G. Mourou, and T. Tajima, *Rev. Accel. Sci. Technol.* **10**, 227 (2019).
2. D. E. Rivas, A. Borot, D. E. Cardenas, G. Marcus, X. Gu, D. Herrmann, J. Xu, J. Tan, D. Kormin, G. Ma, W. Dallari, G. D. Tsakiris, I. B. Foldes, S. W. Chou, M. Weidman, B. Bergues, T. Wittmann, H. Schroder, P. Tzallas, D. Charalambidis, O. Razskazovskaya, V. Pervak, F. Krausz, and L. Veisz, *Sci. Rep.* **7**, 5224 (2017).
3. Z. Li, Y. Kato, and J. Kawanaka, *Sci. Rep.* **11**, 151 (2021).
4. M. L. Zhou, X. Q. Yan, G. Mourou, J. A. Wheeler, J. H. Bin, J. Schreiber, and T. Tajima, *Phys. Plasmas* **23**, 043112 (2016).
5. X. Wu, Z. Gong, Y. Shou, Y. Tang, J. Yu, G. Mourou, and X. Yan, *Phys. Plasmas* **28**, 023102 (2021).
6. D. Papp, Z. Léczy, C. Kamperidis, and N. A. Hafz, *Plasma Phys. Contr. Fusion* **63**, 065019 (2021).
7. Z. Léczy, A. Andreev, D. Papp, C. Kamperidis, and N. A. Hafz, *Plasma Phys. Contr. Fusion* **65**, 105001 (2023).
8. E. Ridente, M. Mamaikin, N. Altwajry, D. Zimin, M. F. Kling, V. Pervak, M. Weidman, F. Krausz, and N. Karpowicz, *Nat. Commun.* **13**, 1111 (2022).
9. T. T. Luu, M. Garg, S. Y. Kruchinin, A. Moulet, M. T. Hassan, and E. Goulielmakis, *Nature* **521**, 498 (2015).
10. S.-W. Huang, G. Cirmi, J. Moses, K.-H. Hong, S. Bhardwaj, J. R. Birge, L.-J. Chen, E. Li, B. J. Eggleton, and G. Cerullo, *Nat. Photonics* **5**, 475 (2011).
11. E. Goulielmakis, M. Schultze, M. Hofstetter, V. S. Yakovlev, J. Gagnon, M. Uiberacker, A. L. Aquila, E. Gullikson, D. T. Attwood, and R. Kienberger, *Science* **320**, 1614 (2008).
12. I. B. Mukhin, A. A. Soloviev, E. A. Perevezentsev, A. Shaykin, V. N. Ginzburg, I. V. Kuzmin, M. A. Mart'yanov, I. A. Shaikin, A. A. Kuzmin, S. Yu. Mironov, I. V. Yakovlev, and E. A. Khazanov, *Quantum Electron.* **51**, 759 (2021).
13. J. Bromage, S.-W. Bahk, I. Begishev, C. Dorrer, M. Guardalben, B. Hoffman, J. Oliver, R. Roides, E. Schiesser, and M. Shoup III, *High Power Laser Sci. Eng.* **7**, e4 (2019).
14. C. Radier, O. Chalus, M. Charbonneau, S. Thambirajah, G. Deschamps, S. David, J. Barbe, E. Etter, G. Matras, S. Ricaud, V. Leroux, C. Richard, F. Lureau, A. Baleanu, R. Banici, A. Gradinariu, C. Caldararu, C. Capiteanu, A. Naziru, B. Diaconescu, V. Iancu, R. Dabu, D. Ursescu, I. Dancus, C. A. Ur, K. A. Tanaka, and N. V. Zamfir, *High Power Laser Sci. Eng.* **10**, e21 (2022).
15. S. Y. Mironov, S. Fourmaux, P. Lassonde, V. Ginzburg, S. Payeur, J.-C. Kieffer, E. Khazanov, and G. Mourou, *Appl. Phys. Lett.* **116**, 241101 (2020).
16. P.-G. Bleotu, J. Wheeler, S. Y. Mironov, V. Ginzburg, M. Masruri, A. Naziru, R. Secareanu, D. Ursescu, F. Perez, and J. De Sousa, *High Power Laser Sci. Eng.* **11**, e30 (2023).
17. G. M. Rossi, R. E. Mainz, Y. D. Yang, F. Scheiba, M. A. Silva-Toledo, S. H. Chia, P. D. Keathley, S. B. Fang, O. D. Muecke,

- C. Manzoni, G. Cerullo, G. Cirimi, and F. X. Kaertner, *Nat. Photonics* **14**, 629 (2020).
18. M. Veinhard, S. Bellanger, L. Daniault, I. Fsaifes, J. Bourderionnet, C. Larat, E. Lallier, A. Brignon, and J.-C. Chanteloup, *Opt. Lett.* **46**, 25 (2020).
19. C. Manzoni, O. D. Mucke, G. Cirimi, S. B. Fang, J. Moses, S. W. Huang, K. H. Hong, G. Cerullo, and F. X. Kartner, *Laser Photonics Rev.* **9**, 129 (2015).
20. A. J. Benedick, J. G. Fujimoto, and F. X. Kärtner, *Nat. Photonics* **6**, 97 (2012).
21. M. Schultze, A. Wirth, I. Grguras, M. Uiberacker, T. Uphues, A. J. Verhoef, J. Gagnon, M. Hofstetter, U. Kleineberg, and E. Goulielmakis, *J. Electron Spectrosc. Related Phenomena* **184**, 68 (2011).
22. L. Lepetit, G. Chériaux, and M. Joffre, *J. Opt. Soc. Am. B* **12**, 2467 (1995).
23. C. Dorrer, N. Belabas, J.-P. Likforman, and M. Joffre, *J. Opt. Soc. Am. B* **17**, 1795 (2000).
24. E. Khazanov, A. Shaykin, I. Kostyukov, V. Ginzburg, I. Mukhin, I. Yakovlev, A. Soloviev, I. Kuznetsov, S. Mironov, A. Korzhimanov, D. Bulanov, I. Shaikin, A. Kochetkov, A. Kuzmin, M. Martyanov, V. Lozhkarev, M. Starodubtsev, A. Litvak, and A. Sergeev, *High Power Laser Sci. Eng.* **11**, e78 (2023).
25. Y. Peng, Y. Xu, L. Yu, X. Wang, Y. Li, X. Lu, C. Wang, J. Liu, C. Zhao, Y. Liu, C. Wang, X. Liang, Y. Leng, and R. Li, *Rev. Laser Eng.* **49**, 93 (2021).
26. V. E. Leshchenko, *Opt. Express* **23**, 15944 (2015).
27. L. Zhang, J. Chen, C. Ma, W. Li, Z. Qi, and N. Xue, *Laser Photonics Rev.* **15**, 2100016 (2021).
28. R. Cheng, C.-L. Zou, X. Guo, S. Wang, X. Han, and H. X. Tang, *Nat. Commun.* **10**, 4104 (2019).